

## Article

# Influence of 1-Ethyl-3-methylimidazolium Diethylphosphate Ionic Liquid on the Performance of Eu- and Gd-Doped Diamond-like Carbon Coatings

Mohammadamin Sadeghi<sup>1</sup>, Takeru Omiya<sup>1,2</sup>, Filipe Fernandes<sup>1,2,3</sup>, Luís Vilhena<sup>1</sup>, Amilcar Ramalho<sup>1</sup> and Fábio Ferreira<sup>1,2,4,\*</sup>

- <sup>1</sup> CEMMPRE, ARISE, Department of Mechanical Engineering, University of Coimbra, Rua Luís Reis Santos, 3030-788 Coimbra, Portugal; masadeghiedu@gmail.com (M.S.); takeru.omiya@student.dem.uc.pt (T.O.); filipe.fernandes@dem.uc.pt (F.F.); luis.vilhena@uc.pt (L.V.); amilcar.ramalho@dem.uc.pt (A.R.)  
<sup>2</sup> Laboratory for Wear, Testing & Materials, Instituto Pedro Nunes, Rua Pedro Nunes, 3030-199 Coimbra, Portugal  
<sup>3</sup> ISEP, Polytechnic of Porto, Rua Dr. António Bernardino de Almeida, 4249-015 Porto, Portugal  
<sup>4</sup> Walker Department of Mechanical Engineering, The University of Texas at Austin, Austin, TX 78712, USA  
\* Correspondence: fabio.ferreira@dem.uc.pt

**Abstract:** A composite lubricating system that combines solid and liquid lubrication can create a synergistic effect by leveraging the strengths of both types of lubricants. Solid lubrication coatings possess advantageous load-bearing abilities and exhibit low volatility. By adopting this approach, the system retains the merits of solid lubrication while simultaneously harnessing the advantages of liquid lubrication. The unique properties of diamond-like carbon coatings (DLCs) offer the potential to create binding locations for lubricant additives by introducing dopant elements that have a high affinity with additives. In the present work, the combined use of europium-doped diamond-like carbon (Eu-doped DLC) with varying atomic concentrations of the dopant element (1.7 at. % and 2.4 at. %) and gadolinium-doped diamond-like carbon (Gd-doped DLC) with different atomic concentrations of the dopant element (1.7 at. % and 2.3 at. %) was studied alongside a pure DLC coating and the incorporation of an ionic liquid (IL) additive in a tribological block-on-ring system. The focus was on the 1-Ethyl-3-methylimidazolium diethylphosphate ionic liquid with a concentration of 1 wt. % in polyalphaolefin (PAO) 8. Among the investigated pairs, the coefficient of friction (CoF) of 1.7 at. % Eu-doped DLC coupled with the IL was the smallest in boundary, mixed, and elastohydrodynamic lubrication regimes. Quantification of wear was challenging due to minimal and localized wear on the DLC coating surfaces. The decrease in friction within the boundary lubrication regime underscores the promise of mechanical systems that integrate 1.7 atomic percent Europium-doped diamond-like carbon coatings with ionic liquids (IL). This study presents a compelling avenue for future scholarly exploration and research efforts focused on reducing friction and improving the efficiency of moving components, particularly in situations where tribological properties exert a substantial influence

**Keywords:** lubricant additives; DLC; lubrication regime; tribology; thin film



**Citation:** Sadeghi, M.; Omiya, T.; Fernandes, F.; Vilhena, L.; Ramalho, A.; Ferreira, F. Influence of 1-Ethyl-3-methylimidazolium Diethylphosphate Ionic Liquid on the Performance of Eu- and Gd-Doped Diamond-like Carbon Coatings.

*Lubricants* **2024**, *12*, 18. <https://doi.org/10.3390/lubricants12010018>

Received: 27 October 2023

Revised: 1 January 2024

Accepted: 5 January 2024

Published: 8 January 2024



**Copyright:** © 2024 by the authors. Licensee MDPI, Basel, Switzerland. This article is an open access article distributed under the terms and conditions of the Creative Commons Attribution (CC BY) license (<https://creativecommons.org/licenses/by/4.0/>).

## 1. Introduction

The urgent requirement to decrease greenhouse gas emissions necessitates innovative measures to positively influence our planet's condition in the coming years. Control of friction elements plays a direct role in enhancing the performance of systems by minimizing heat dissipation and reducing wear. This, in turn, enables significant energy preservation throughout the lifespan of the system. Effective friction management further extends the durability of components by reducing undesirable deterioration, leading to favorable energy conservation outcomes through the diminished necessity for component replacements [1–3]. Therefore, currently, there is a huge emphasis on creating advanced materials

that can effectively reduce friction and enhance the durability of mechanical components in motion. To comprehensively explore this, significant studies in tribology are trying to understand how lubricants impact the behavior of moving parts. It is crucial to recognize that friction and wear are attributes of the entire system, not just the materials involved. Promising solutions include the utilization of ILs as additives to lubricants and thin DLC coatings [4]. Previous research works have proven the benefits of utilizing DLCs, ILs, or base lubricants alone or simultaneously to minimize friction or wear.

Lubricant additives are extensively utilized to amplify existing attributes or introduce supplementary tribological characteristics. These additives encompass chemical compounds capable of engaging with surfaces, resulting in the development of layers with diminished shear strength resistance, commonly termed as “tribofilms” [5].

Zinc dialkyl dithiophosphates (ZDDPs) have found application as additives within formulations of engine oils, a practice dating back to the 1940s. Their primary purpose has been to mitigate the effects of wear [6]. Extensive research has been dedicated to understanding the lubrication mechanism of ZDDP over the course of numerous years. The prevalent theory explaining how ZDDP reduces wear involves the development of uneven glassy phosphate coatings on surfaces. Despite their remarkable effectiveness in diverse conditions, these additives contain notable amounts of phosphorus, sulfur, and zinc. These elements are suspected culprits behind issues like filter blockages and catalyst deterioration within post-combustion treatment processes for car engines. Consequently, the environmental drawbacks linked to ZDDP application have drawn intensified criticism. This has prompted active exploration into alternative solutions to replace ZDDPs [6–8], giving precedence to the development of environmentally friendly biodegradable lubricants with diminished toxicity levels.

Numerous research endeavors have explored the incorporation of diverse metallic elements into DLC films, aiming to elevate their attributes and primarily rectify certain undesirable characteristics achieving beyond the already commendable tribological and mechanical capabilities exhibited by DLC coatings [9]. Commonly, properties of diamond-like carbon films are modified using two primary groups of alloying materials: non-carbide formers (such as copper and silver) and carbide formers (e.g., titanium, chromium, tungsten) [10–16].

Elevated residual stress within DLC films can result in inadequate adhesion, potentially leading to coating delamination, even during the process of film deposition. This observation is supported by multiple research studies [17–21]. The incorporation of metallic or non-metallic elements as dopants offers a means to diminish residual stress by regulating the microscopic arrangement, adhesion,  $sp^3/sp^2$  ratio, and surface texture of DLC coatings. Consequently, the capacity to control the carbon bond structure and minimize residual stress emerges as a pivotal element for achieving the desired properties within a DLC film [19]. To minimize residual stress, DLC coatings have been doped with Ti [22,23], W [19,24], Si [25], N [26], F [21], Nb [18], and Au [17]. Doping additionally enhances the efficacy of thin DLC films in the realm of biomedical applications, such as for ureteral stents [27]. In the domain of hospital-utilized instruments necessitating antibacterial qualities, the addition of substances like Ag into DLC confers this specific attribute [14,28].

Among numerous suggested solutions to supplement or substitute ZDDPs, ILs have garnered significant interest from the research community. ILs consist of an anion and an organic cation, constituting liquid salts with melting points below 100 °C [29,30]. In many ILs, the absence of metallic elements does not preclude their interaction with metal substrates or the debris they produce.

In this research study, 1-Ethyl-3-methylimidazolium diethyl phosphate was selected as an additive to PAO8. This particular ionic liquid exhibited superior lubricating properties compared to polyalphaolefin, effectively reducing friction. Nanao et al. [31] examined the tribological characteristics of 1-Ethyl-3-methylimidazolium diethyl phosphate at room temperature. The mentioned IL was discovered to exhibit superior lubricating properties, effectively reducing friction compared to polyalphaolefin.

Several research studies have investigated the incorporation of dopant elements in DLC coating to improve their tribological efficacy when exposed to ILs. In a study by Milewski et al. [32], the tribological performance of two distinct ionic liquids (named as 1-butyl-3-methylimidazolium tetrafluoroborate and trihexyltetradecylphosphonium bis(trifluoromethylsulfonyl) amide) was examined on an a-C:H type diamond-like carbon coating deposited on a 100Cr6 steel disk which was sliding against a 100Cr6 steel ball under a boundary lubrication regime. The specimens coated with a-C:H type diamond-like carbon and lubricated with 1-butyl-3-methylimidazolium tetrafluoroborate ionic liquid exhibited the lowest friction value among all observed values.

Gonzalez et al. [33] investigated the effectiveness of a chromium-doped DLC coating used in a system lubricated with two different ionic liquids named as ethyl-dimethyl-2-methoxyethylammonium tris(pentafluoroethyl)trifluorophosphate [(NEMM)MOE] [FAP] and 1-butyl-1-methylpyrrolidinium tris(pentafluoroethyl)trifluorophosphate [BMP] [FAP]. These ionic additives had concentrations of 1 wt% in a polyalphaolefin base oil. The study revealed that both ionic liquids helped to decrease friction, particularly noticeable at the lowest tested load (20 vs. 40 N).

In other studies [34,35] researcher conducted a study examining the friction and wear interactions between three distinct ILs and a type of W-DLC coating. The ionic liquids studied were Tributylmethylphosphonium dimethylphosphate, trimethylammonium dimethylphosphate, and 1-butyl-1-methylpyrrolidinium tris(pentafluoroethyl)trifluorophosphate ([BMP][FAP]). When applied to the surface of tungsten-doped DLC (W-DLC), the IL additives containing dimethylphosphate anions displayed a noteworthy performance, surpassing even the ZDDP performance under experimental conditions. In contrast, the IL containing the trifluorophosphate group exhibited the least favorable properties among all the ILs tested against W-DLC surfaces.

Khanmohammadi and colleagues [5] undertook a comprehensive examination of the tribological performance involving three categories of diamond-like carbon coatings (DLCs): pure DLC, tungsten-doped DLC, and silver-doped DLC. These DLCs were tested in conjunction with three distinct groups of ionic liquids, namely tributylmethylphosphonium dimethylphosphate (PP), 1,3-dimethylimidazolium dimethylphosphate (IM), and 1-butyl-1-methylpyrrolidinium tris(pentafluoroethyl)trifluorophosphate. They identified two distinct additive-adsorption mechanisms that predominantly influence the frictional characteristics. In the case of Ag-DLC, an activation process involving triboelectrochemical phenomena was observed, whereas in W-DLC, a mechanism involving electron transfer was identified. Both mechanisms led to a significant reduction in friction during contact, providing insights into the efficient friction reduction achieved in these systems.

PAO 8, a prominently branched lubricant, has been subject to several studies aimed at enhancing its tribological effectiveness when employed to lubricate DLC coatings. Lanthanides, encompassing elements such as europium and gadolinium, are regarded as exerting a beneficial influence on the development of tribolayers when utilized as additives in conjunction with ILs. This is attributed to their notable affinity for ionic liquids, which enhances their potential for enhancing tribological interactions [36,37]. These coatings, renowned for their advantageous tribological characteristics, find widespread application in the automotive sector [38]. Conversely, while earlier research has demonstrated the strong chemical attraction of lanthanides, such as europium (Eu) and gadolinium (Gd), towards ILs, and in certain instances, ILs have been employed in the extraction of rare earth metals, the potential benefits of leveraging this affinity to enhance the tribological interplay between ILs and La-DLC films have not been comprehensively explored [36,37,39]. Therefore, this research initiative investigates the influence of introducing europium (Eu) and gadolinium (Gd) dopants into DLC coatings, fabricated through HiPIMS. The primary focus is on comprehending the tribological relationships between these doped diamond-like carbon films with a newly formulated IL called 1-Ethyl-3-methylimidazolium diethylphosphate. To facilitate this study, 1-Ethyl-3-methylimidazolium diethylphosphate is introduced as an additive (1 wt. %) to polyalphaolefin 8 (99 wt.%), serving as the fundamental base

oil. The investigation of tribological performance is conducted under varying lubrication conditions, achieved by modifying the rotational speed of the ring component within a block-on-ring setup (at room temperature). The outcomes are subsequently compared with samples lubricated solely with the base oil (without additives). The objective is to underscore the advantages of incorporating two rare earth elements (Gd and Eu) into diamond-like carbon films in relation to the tribological behavior of DLCs in the presence of 1-Ethyl-3-methylimidazolium diethylphosphate, an additive to PAO8—a lubricant commonly employed in car engines [2]. If further investigations are performed (such as corrosion characterization), the outcome of the present work can be applied in internal combustion engines.

## 2. Materials and Methods

### 2.1. Preparing Samples

The substrate material chosen for the DLC film was an AISI M2 steel, characterized by a coin shape with 12.5 mm radius and 4 mm thickness. Silicon wafers sized 20 × 20 mm and 1 mm thick were chosen for analyzing the film characteristics, namely, the film thickness and morphology. The M2 steel specimens were polished using abrasive grinding papers of varying grit sizes: 240-, 320-, 400-, 600-, 800-, and 1200-grit. For achieving a polished mirror finish ( $R_a \approx 0.1 \mu\text{m}$ ), a paste containing diamond abrasive particles (6 and 3  $\mu\text{m}$ ) was applied. A meticulous cleaning process involving multiple ultrasonic baths with acetone and after ethanol, each lasting for 15 min, was carried out for all substrates [2,9]. Chemical composition of AISI M2 Steel is depicted in Table 1.

**Table 1.** Chemical composition of AISI M2 Steel.

Material	Fe	C	Cr	Mo	W	V
M2 Steel (wt. %)	Balance	1.0	0.4	5.0	6.0	2.0

### 2.2. Coatings Deposition

The DLC film production was carried out by magnetron sputtering with a HiPIMS Cyprium plasma generator, provided by Zpulsor Inc. Throughout the deposition, the substrate holder support rotated at a consistent rate of 23.5 revolutions per minute. The distance between the substrates and the targets was consistently maintained at 80 mm. Two targets were employed, chromium (99.99% purity) and graphite (99.95% purity), measuring 150 × 150 × 10 mm<sup>3</sup>. These targets were responsible for depositing the adhesion interlayers and the diamond-like carbon films, respectively. The pure graphite target underwent modification by introducing circular grooves with a diameter of 10 mm and a depth of 2 mm. These grooves were designed to accommodate doping pellets (either gadolinium or europium pellets) as targets for deposition. In cases where non-doped diamond-like carbon coatings were being deposited, the mentioned holes were filled with graphite pellets to create a pure carbon target.

A base pressure of  $3.0 \times 10^{-5}$  Pa was achieved before the production of all coatings. Improving the adherence of the diamond-like carbon coatings to the substrates involved applying two interlayers before the final diamond-like carbon coating. The process initiated with an interlayer of chromium (Cr), proceeded by an interlayer of chromium nitride (CrN).

The three primary steps of the deposition procedure were as follows:

1. Etching process: Cleaning of the C target involved applying a HiPIMS charging voltage of 400 V at a working pressure of  $4.0 \times 10^{-1}$  Pa for a duration of 10 min. A similar cleaning procedure was carried out on the Cr target, using a DC power of 250 W at a working pressure of  $3.5 \times 10^{-1}$  Pa. Simultaneously, the substrates were subjected to pulsed power (120 kHz, 1616 ns) for 60 min.
2. Interlayer deposition: The chromium (Cr) interlayer was deposited at a working pressure of  $3.0 \times 10^{-1}$  Pa, with a bias of  $-60$  V and a DC power of 1200 W applied to the Cr target. This step lasted for ten minutes. The gas composition was gradually

adjusted by increasing the percentage of nitrogen ( $N_2$ ) and reducing the percentage of argon (Ar) to facilitate the deposition of the CrN layer. Both interlayers had a thickness of approximately 400 nm.

3. DLC coating deposition: The final step involved depositing the DLC coating for 60 min at a pressure of  $4 \times 10^{-1}$  Pa. The deposition procedure utilized micro-pulsing with a duration of 6  $\mu s$  for each micro-pulse, separated by intervals of 150  $\mu s$ . The entire pulse cycle spanned 1800  $\mu s$ . A substrate voltage bias of  $-80$  V was applied, and the average power was maintained at 600 W. Figure 1 presents an overview of the deposition procedure [2].

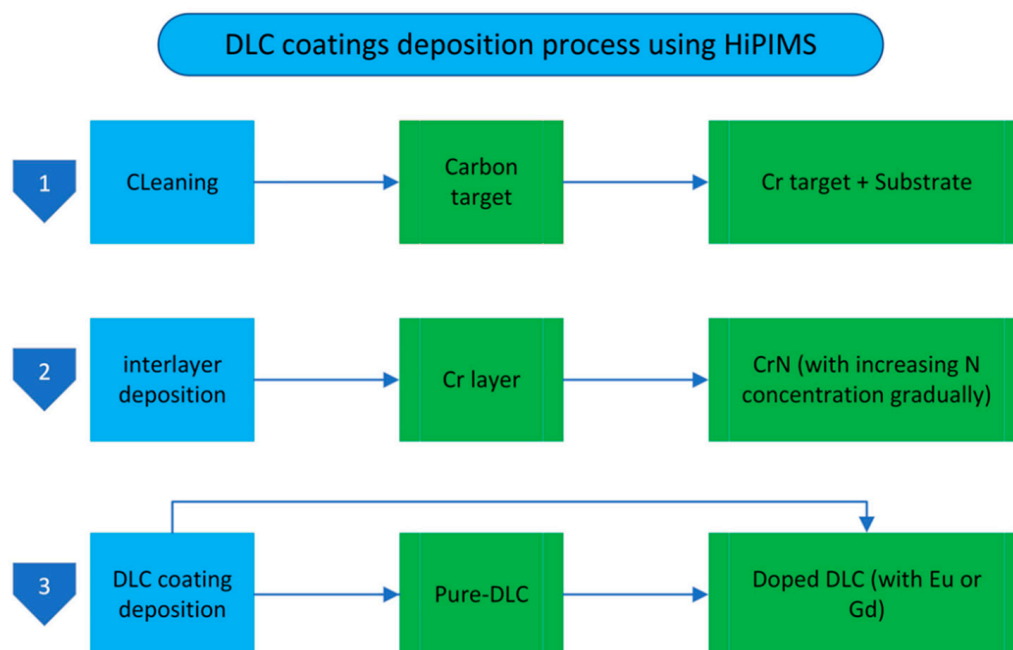


**Figure 1.** An overview of the deposition procedure. (Numbers show the steps followed sequentially).

### 2.3. Lubricants

To comprehend the influence of introducing Gd and Eu elements into DLC films, an initial investigation utilized a basic lubricating oil devoid of any additives. Subsequently, this base oil was mixed with IL additives to observe how the films responded when exposed to an oil blend containing these additives. The primary objective of this research was to analyze the tribological aspects, including friction, wear, and lubrication behavior, of the DLC coatings under these compound lubricating conditions. Within the context of car engines, interactions between the piston ring and cylinder liner primarily occur in two lubrication states: hydrodynamic lubrication and mixed lubrication. Typically, during the piston's motion, mixed and hydrodynamic lubrication states predominate. However, at the upper limit of the piston stroke, the boundary lubrication state becomes notably more significant. This specific condition underscores the necessity for specialized coatings to enhance lubrication. The chosen lubricant for the study was a commercial oil named polyalphaolefin 8 (PAO 8). This selection was made based on the fact that PAO 8 serves as a foundational oil in various commercial engines. Additionally, it has been extensively researched and serves as a reference in numerous scientific studies [2]. The utilization of this base lubricating oil, both in its pure form and in combination with additives, allowed for a comprehensive analysis of the coatings' performance throughout various lubrication conditions [40–42]. For the purposes of this research, the IL known as 1-Ethyl-3-methylimidazolium diethylphosphate was employed. To formulate the lubricant mixture, 1 g of this specific ionic liquid was carefully combined with 99 g of polyalphaolefin 8. This blending process resulted in the development of a lubricant solution containing

1 wt. % of 1-Ethyl-3-methylimidazolium diethylphosphate [2]. The volume of lubricants was 100 mL.

#### 2.4. Characterization Methods

Nano-indentation measurements were employed as a technique to obtain the reduced Young's modulus and hardness of the material. This process involved the utilization of a nano-indenter equipped with a Berkovich indenter. To ensure accurate results, it was essential to keep the depth of indentation minimal, specifically less than 10% (a maximum load of 0.01 N was applied) of the coating's thickness. For every sample, sixteen assessments at different points were conducted. These evaluations aimed to establish both the mean value and the standard deviation of the acquired parameters. This comprehensive approach allowed for a robust understanding of the material's mechanical properties through multiple data points and statistical analysis [2,43,44].

The elemental composition of the doped-DLC films underwent analysis on the Synthesis, Irradiation and Analysis of Materials platform (SIAM), utilizing ERD (Elastic Recoiling Detection) and RBS (Rutherford Backscattering Spectrometry) techniques. The specimen's positioning, alpha beam examination, data processing, and cross-section function measurements were all integral steps in analyzing the thin film's elemental composition and characteristics. To perform the evaluation, the sample was inclined at an angle of 70° and subjected to an alpha beam analysis at an energy level of 2.3 MeV. Throughout this process, backscattered particles were collected using a stationary detector positioned at a 30° angle relative to the incident beam's path. Comprehensive elemental depth profiles were generated by processing the collected data using Data Furnace [45]. Specifically, five spectra were recorded for each specimen, and cross-section functions were measured through the application of SigmaCalc data. SigmaCalc data were employed for determining cross-section values [2,46].

Scanning electron microscopy (SEM), using the Zeiss Merlin equipment, was carried out to investigate the morphology and the thickness of the DLC films, obtained from the surface area and a cross-section, respectively. The SEM images were achieved with a 2 keV electron high tension (EHT) voltage.

Raman spectroscopy, a non-destructive method, was used to examine the coating's structure, namely the graphitization of DLC. The spectra were collected using a Renishaw inVia microRaman equipped with a He-Cd laser at 442 nm. For all measurements, the spectral range was 50 to 4000  $\text{cm}^{-1}$ . In this investigation, Raman spectra were obtained at many locations to check for surface heterogeneity. Following the elimination of the linear background, peak fitting was conducted using Gaussian synthetic curves.

The SV-100 A&D viscometer instrument (A&D, Tokyo, Japan) was employed to gauge the viscosity–temperature–time properties of the lubricant, which works based on the tuning-fork vibration functions. This technique relies on an electromagnetic force to induce oscillations in a pair of slender sensor plates, which share similar natural frequencies. These plates vibrate with a designated amplitude in the viscometer based on the tuning-fork concept. By monitoring the electronic current required to maintain the sensor plates at a consistent amplitude, the viscosity of the sample liquid was determined. The sensor plates are characterized by extremely low thermal capacity, and the sample liquid's movement is minimal. This design feature helps prevent fluctuations in the temperature and physical characteristics of the sample. For this research work, the viscosity value determination of two distinct lubricants was conducted at room temperature. Before conducting the tests, the viscometer was calibrated in accordance with the manufacturer's guidelines. Furthermore, the container employed for the samples was meticulously cleaned using ethanol liquid and acetone liquid, followed by thorough drying. This precautionary measure was taken to prevent any potential contamination that could adversely impact the viscosity measurements.

### 2.5. Tribotest

The tribological testing was conducted using a block-on-ring setup (Table 2) according to ASTM G77-17, which mimicked a linear contact geometry [47]. The experimental setup consisted of a power supply, a sample holder, an oil reservoir, a counter body (a ring in this case), and two sensors for real-time force measurements. One sensor quantified the normal force, while the other measured the tangential force. Following Amontons' 1st law, the tangential force demonstrated a direct proportionality to the normal force, where the coefficient of friction (CoF) represented the constant of proportionality. To maintain lubrication between the surfaces, a lubricant reservoir ensured complete submersion. The opposing surface was a ring made of steel (AISI 3415), measuring 115 mm in diameter and 12 mm in width. This steel ring underwent a polished surface treatment using 2000-grit sandpaper to replicate the typical surfaces found in car engines. For the testing conditions, a normal load of 25 N was applied. This load determination followed the principles of Hertzian contact theory, taking into account the specific contact geometry and recognizing the typical pressure of car engines, which is approximately 40 MPa. Block-on-ring tests were performed using different angular speeds corresponding to linear sliding speeds of 0.02, 0.05, 0.07, 0.13, 0.18, 0.4, and 0.66 m/s, respectively. This choice allowed for relevant and practical testing within the context of engine operation (covered all different lubrication regimes), and tests were performed once for every presented velocity, beginning with the highest velocity and ending in the lowest velocity. Figure 2 shows the block-on-ring setup employed in this research work [48], and Figure 3 indicates a detailed image of the block-on-ring contact geometry.

**Table 2.** Information about the counterpart (ring) used in this work.

Properties of the Counterpart (Ring)	
Material	AISI 3415 steel
Diameter	115 mm
Width	12 mm
Young's modulus	205 GPa
Poisson's ratio	0.285

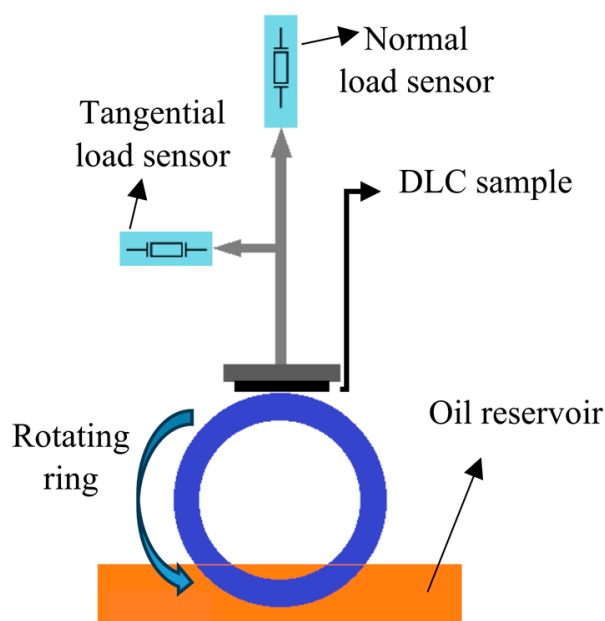


**Figure 2.** Block-on-ring setup used in this work.

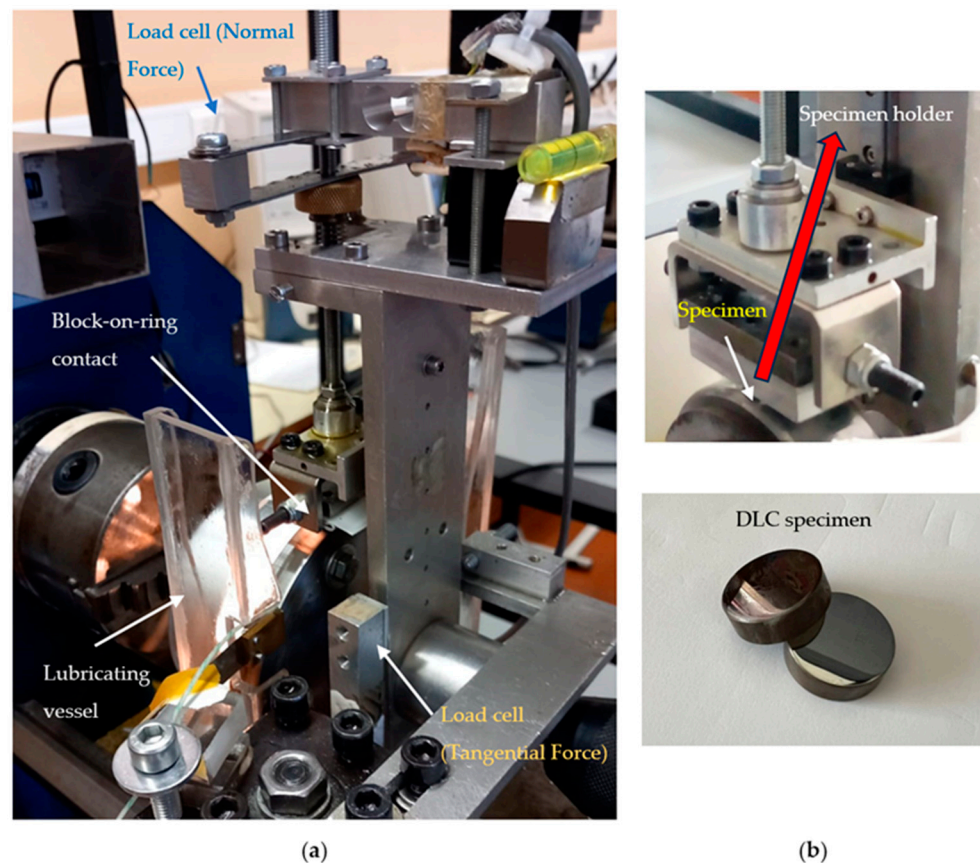


**Figure 3.** Image of the tribometer used during experiments with the two different load cells: (a) global view; (b) detail of the block-on-ring contact geometry.

Hitachi SU-3800 Scanning Electron Microscope (SEM) equipped with Energy-Dispersive X-ray Spectroscopy (EDS) was employed to characterize the wear in the samples after tribology tests. The EDS enables the identification of dissimilar elements [2,49].

### 3. Results and Discussion

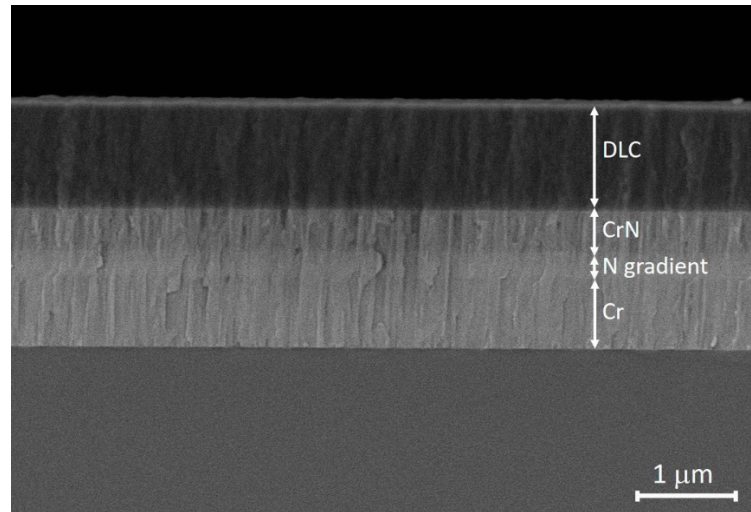
#### 3.1. Chemical Composition, Structure, Hardness, and Reduced Young's Modulus of Thin Films

The findings from the RBS and ERD examinations are detailed in Table 3. According to these results, Gd-doped DLCs consist of approximately 1.7 atomic percent (at. %) and 2.3 at. % of the doped element, while Eu-doped DLCs contain about 1.7 at. % and 2.4 at. % of Eu. Previous studies have proposed that elevated concentrations of Eu and Gd in doped diamond-like carbon films could potentially have adverse effects on the properties of the DLC coating [9]. For instance, an increase in Gd concentration has demonstrated the ability to lower the adhesion properties and hardness values when it comes to Gd-doped DLC. To mitigate these potential negative impacts, this study opted for coatings with low doping element concentrations (lower or equal to 2.4% at. of the dopant element). It is important to note that the presence of hydrogen in the samples is attributed to contamination that cannot be eliminated by vacuum pumps [2,9].

The image depicted in Figure 4 illustrates the cross-sectional scanning electron microscope (SEM) representation of either pure DLC or doped-DLC samples. This visual aid enables the clear observation of the coating's four discernible sections (comprising the interlayers and DLC thin film) formed atop the substrate.

**Table 3.** Elemental composition of different DLC specimens.

Specimen	Chemical Composition (at. %)			
	H	Ar	Gd	Eu
Pure DLC (or DLC)	6.5	3.6	0	0
1.7% Gd-doped DLC	5.8	4.3	1.7	0
2.3% Gd-doped DLC	3.1	2.3	2.3	0
1.7% Eu-doped DLC	8	3.4	0	1.7
2.4% Eu-doped DLC	5.9	3.7	0	2.4

**Figure 4.** Showcases the cross-sectional profile delineating the pure DLC sample, delineating the presence of Cr and CrN interlayers along with the gradient of nitrogen distribution between these layers.

The identical profile morphology, characterized by a columnar microstructure spanning the entire film, persists across all examined samples, irrespective of the doping element type and its atomic concentration. Within the films, an orderly arrangement of alternating dark and bright bands is discernible. The initial three layers, developed above the substrate, consist of a chromium layer, succeeded by a region with a gradient of nitrogen resulting from the establishment of the interlayers, and proximal to this region lies the chromium nitride layer. Concluding this stratified structure is the topmost layer—a thin DLC film. The Cr and CrN interlayers, deposited onto the Si (100) substrate, measure approximately 900 nm in thickness, while the DLC thin film maintains a consistent thickness of roughly 700 nm across all samples.

The Cr and CrN interlayers exhibit an open columnar microstructure known for inducing tensile stresses [50], which serve to counterbalance the compressive stress generated subsequent to the deposition of the DLC coating [51]. This consistent pattern of structural composition and stress distribution is observed consistently throughout the analyzed samples.

The surface morphologies of DLC coatings, deposited by HiPIMS, are shown in Figure 5 as a function of the dope element and atomic concentration.

The consistent presence of cauliflower-like topography was evident across all film specimens, with the sizes of these granules within surface agglomerates exhibiting an incremental growth corresponding to higher atomic concentrations of doping elements. Specifically, in samples doped with elevated atomic percentages of Gd (2.3 at. %), the nodular size surpassed that of undoped DLC or DLC doped with lower atomic concentrations. In the case of Eu-doped samples, their morphology closely resembled those with lower Gd content, aligning with similar patterns observed in the lower concentration Gd samples. These findings strongly suggest that the concentration of the dopant significantly influences the resultant surface morphology variations in doped-DLC films.

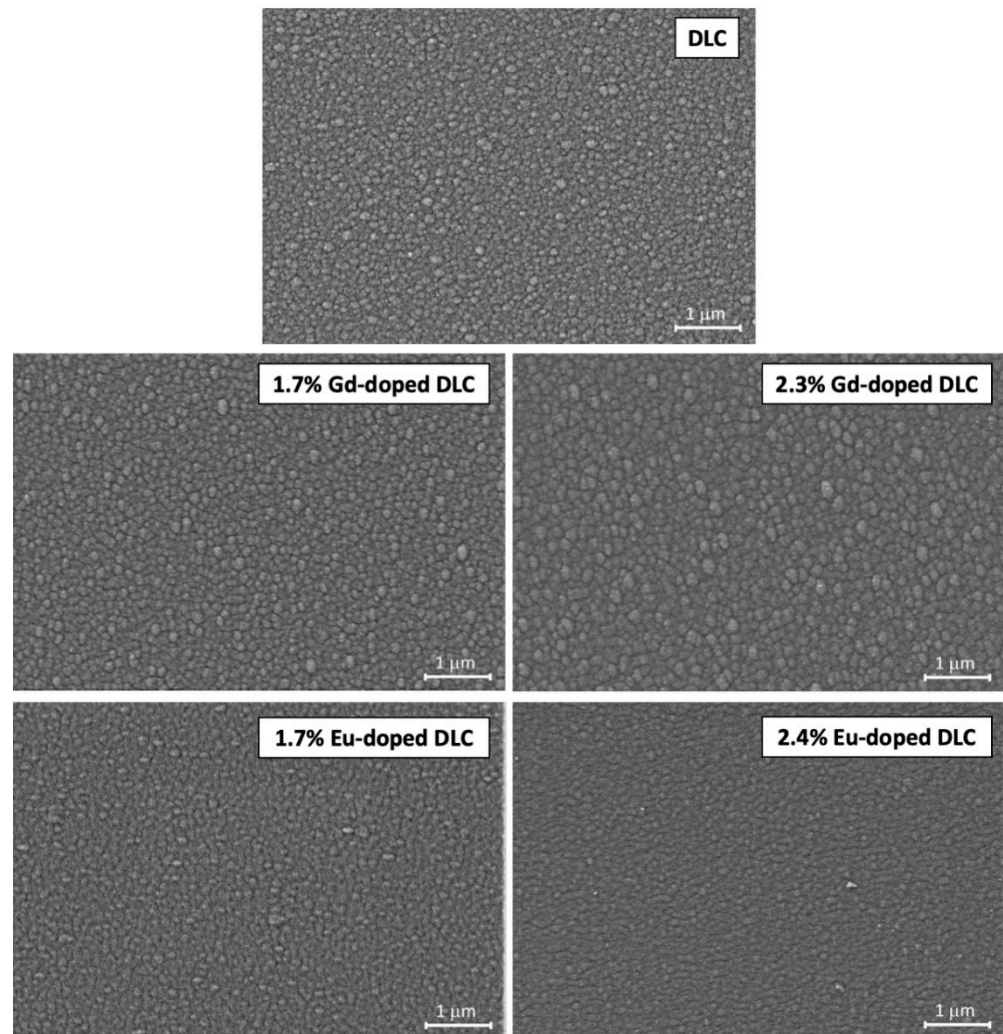


**Figure 5.** The SEM surface morphology of pure-DLC, Gd-, and Eu-DLC.

As outlined by Lin et al. [52], Hatem et al. [53], and Sharifahmadian et al. [54], the size of nodules has a discernible impact on film density, with smaller nodules yielding denser films. Samples such as pure DLC or doped-DLC featuring lower atomic concentrations exhibit denser coatings characterized by increasingly compacted columnar microstructures.

The densification of films leads to noteworthy enhancements in properties such as hardness and wear resistance [51,55–57]. This disparity observed in film density directly correlates with the quantity of  $sp^2$  and  $sp^3$  hybridized bonds present, which significantly govern and delineate the properties of DLC coatings [38,58].

Raman spectroscopy served as the method to investigate the structure of C-based coatings. A widely accepted approach within the research community working on thin-film carbon was employed that displays two primary peaks: the D-peak approximately at  $1350\text{ cm}^{-1}$  and a G-peak around  $1580\text{ cm}^{-1}$ . These peaks correspond, respectively, to the stretching of  $sp^2$  clusters and the in-plane C-C stretching mode of  $sp^2$  hybridized carbon atoms [59].

To interpret the Raman spectra, the D and G bands were meticulously analyzed using a two-peak Gaussian peak fitting method, considering a spectral range between approximately  $1000$  and  $1800\text{ cm}^{-1}$ , aligning with the methodologies described in the study conducted by Schmidt et al. [60].

Various studies have established a correlation between the intensity of the D peak ( $I_D$ ) and the intensity of the G peak ( $I_G$ ) with the concentration of  $sp^3$ , wherein a lower  $I_D/I_G$  value signifies a higher proportion of  $sp^3$  content within a DLC film. As outlined

in Table 4, an increase in the dopant fraction resulted in a rise in the  $I_D/I_G$  ratio of pure DLC, escalating from 0.73 to 0.88 for Gd and to 0.80 for Eu. Although limited studies focus on incorporating lanthanides as dopants in DLC films, Foong et al. [59] observed a similar trend in their research.

**Table 4.** The positioning and magnitudes of the D and G peaks, coupled with the comparative intensity ratio between these peaks are outlined for Gd-DLC and Eu-DLC coatings.

DLC Samples	$x_D$	$I_D$	$x_G$	$I_G$	$I_D/I_G$
Pure DLC	1367	1110.2	1554	1511.6	0.73
1.7% Gd-DLC	1387	1223.7	1547	1501.8	0.81
2.3% Gd-DLC	1376	995.5	1536	1133.4	0.88
1.7% Eu-DLC	1376	1443.9	1556	1826.1	0.79
2.4% Eu-DLC	1370	1304.8	1530	1641.3	0.80

The evaluations of Young's modulus ( $Y$ ) and hardness ( $H$ ), as illustrated in Figure 6, indicate that both the 1.7% Gd-doped diamond-like carbon coating and the pure diamond-like carbon coating demonstrate enhanced hardness in comparison to the other coatings, considering the margin of error represented by the error bars. Similarly, in terms of Young's modulus, both 1.7% Gd-doped DLC and pure DLC display the highest values for this property, considering the variability indicated by the error bars. DLC coatings are primarily composed of two types of carbon bonds, resembling the hybridizations found in both graphite (addressed as  $sp^2$  hybridization) and diamond (addressed as  $sp^3$  hybridization). This unique combination contributes to the exceptional  $H$  and  $Y$  observed in DLC. However, it is important to note that diamond-like carbon films are also characterized by relatively high stresses [61,62]. In the literature, some characteristics are linked to the prevalence of  $sp^3$  hybridization within the films. Research indicates that as the proportion and density of  $sp^3$  hybridization increase, so do the levels of hardness. Enhanced hardness of surfaces leads to increased resistance against abrasive wear [9,16,38,63–65]. If 1.7% Gd-doped DLC and 2.3% Gd-doped DLC are compared, note that the hardness values and elasticity modulus decrease as the percentage of the dopant element increases [2].

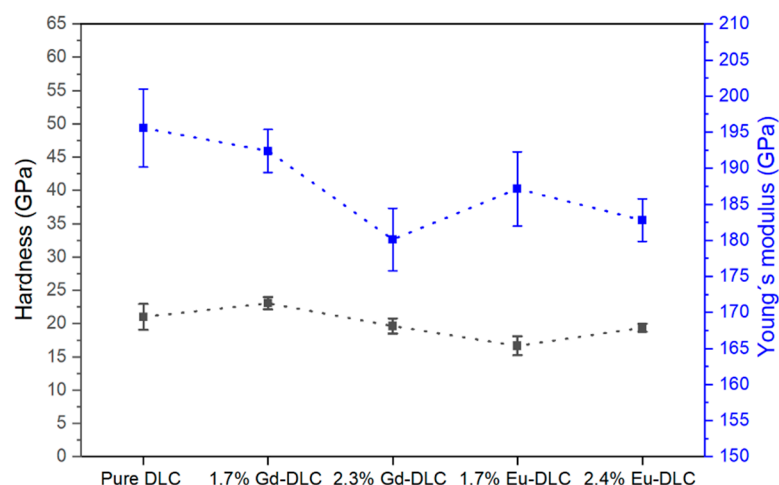


**Figure 6.**  $H$  and  $Y$  of the diamond-like carbon films. (The purpose of the lines connecting the measured points is to provide visual guidance for the reader, without representing any specific measured values or a continuous trend).

### 3.2. Lubricant Viscosity

Table 5 presents the viscosity data for the employed lubricants. The results indicate that the incorporation of the IL additive into polyalphaolefin 8 did not bring about a significant change in viscosity. The viscosity of Newtonian fluids plays a crucial role as

a transitional factor in the lubrication regime. In the experiments conducted, an increase in viscosity caused a transition in the lubrication state toward the hydrodynamic phase. As a result, under the same sliding velocity, the film thickness expanded in comparison to polyalphaolefin 8 without additives [2].

**Table 5.** Values of viscosity at room temperature for various lubricants.

Lubricant	Dynamic Viscosity (mPa·s)	Kinematic Viscosity (mm <sup>2</sup> /s)
PAO 8	71.89	86.48
PAO 8 + additive (1 wt. %)	76.89	92.49

### 3.3. Stribeck Curves

Stribeck curves (SC) are illustrated by graphing the CoF against the Hersey number or  $\lambda$  (lambda ratio, which is a metric employed to characterize the lubrication regime). The Hersey number, a dimensionless quantity, is computed as the product of the dynamic viscosity of the lubricant ( $\eta$ ) and the linear speed ( $u$ ), divided by the applied load ( $P$ ) per unit of contact length ( $m$ ). In the context of these experiments, as velocity was the sole variable, fluctuations in the Hersey parameter were solely influenced by changes in the sliding speed. The applied load remained consistently around 25 N throughout all of the experiments [48,66,67].

Figure 7 illustrates the SC derived from experimental data gathered at varying velocities. According to the figure, four distinct lubrication regimes can be identified [2,40,68].

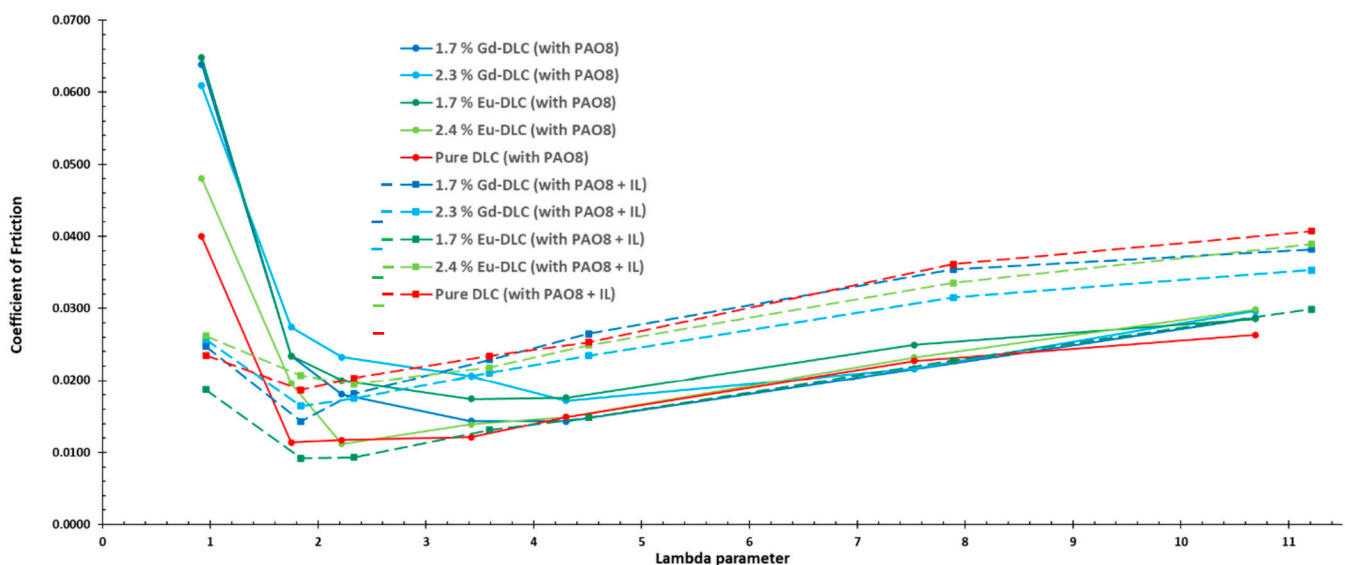


**Figure 7.** SC obtained for polyalphaolefin 8 and polyalphaolefin 8 with IL additive for various DLC specimens. (The purpose of the dashed lines connecting the measured points is to provide visual guidance for the reader, without representing any specific measure).

In the boundary lubrication (BL) regime, characterized by  $\lambda < 1$ , the load is borne by the microscopic surface irregularities, as there is no continuous lubricating film [2,66,68–72]. The intermediate state, termed mixed lubrication (ML) within the parameter range of  $1 < \lambda < 3$ , combines attributes from both elastohydrodynamic lubrication (EL) and BL. This means that while some regions of the contact area benefit from a lubricating film, other areas involve the interaction between surface imperfections, lacking a continuous liquid film to separate them [2,69,71]. In the EL condition, the lubricating film thickness is significantly reduced compared to the hydrodynamic regime (HL) [2,68,69,73]. Extending beyond HL, the EL condition ( $3 < \lambda < 5$ ) involves the deformation of the contacting surfaces. Finally, in the HL regime (where  $\lambda > 5$ ), the entire load is supported by the lubricant film [2,66,68–73].

Upon scrutinizing the SC of different DLC films, it was observed that the addition of the IL to the polyalphaolefin 8 lubricant typically led to a reduction in the CoF at the minimum attainable sliding velocity in the employed tribometer (which falls within the boundary regime in this example). This effect was particularly noticeable in the case of 1.7 atomic % Eu-doped DLC. When evaluating the tribological pairs lubricated with polyalphaolefin 8 + 1 wt. % additive, as illustrated in Figure 5, a distinct alteration in the CoF becomes apparent across all pairs in the BL regime. Remarkably, within this regime, the 1.7% Eu-doped DLC coating exhibits superior performance compared to all other coatings. In both the EL and HL regimes, the CoF for coatings like pure DLC, 1.7% Gd-doped DLC, 2.3% Gd-doped DLC, and 2.4% Eu-doped DLC, when coupled with polyalphaolefin 8 + 1 wt. % additive, shows higher values in contrast to the same coatings coupled with pure polyalphaolefin 8. However, the performance of 1.7% Eu-doped DLC coupled with polyalphaolefin 8 + 1 wt. % additive remains comparable to the DLC coatings coupled with pure polyalphaolefin 8, particularly in mixed and elastohydrodynamic lubrication regimes.

In the previous reviews [74], two mechanisms have been proposed to explain how the use of ILs additives can reduce the CoF. One is the capability to facilitate motion since they possess small values of shear stress resistance. In this mechanism, the anionic constituent of an ionic liquid is attracted to the surface which usually has positive charges, resulting in the adsorption of these ions onto the surface [74]. Subsequently, the cationic element can bind to another anionic element, giving rise to the buildup of single or multi-layer adsorbed configurations on the surface. These configurations create a layer over the contact surface characterized by feeble interlayer forces. This quality contributes to the reduction of friction and facilitates the motion between the interacting surfaces [5,75–77]. The second mechanism explored in the literature pertains to the formation of a tribofilm on surfaces. These separating layers are generated through chemical reactions occurring between the components of IL and wear particles generated in contact, serving to protect and reduce wear [5,70,75].

The Higginson [78] equation is employed to compute the minimum film thickness ( $h_0$ ) and the  $\lambda$  value (the ratio of  $h_0$  to composite surface roughness). These calculated values are presented in both Tables 6 and 7. For both lubricants, the lubrication condition commences from a fully hydrodynamic state. As the velocity decreases, the  $\lambda$  ratio also diminishes, eventually transitioning to the BL condition. In this latter stage, the surfaces come into direct contact without a lubricant film between them, potentially resulting in the wear and degradation of both surfaces. Importantly, due to the higher viscosity of the polyalphaolefin 8 + 1 wt. % additive, the film thickness in this scenario is increased, causing a slight rightward shift of the entire curve. This modification leads to a relatively prolonged hydrodynamic regime [2].

**Table 6.** Characteristics of lubrication film for polyalphaolefin 8 based on the velocity of the cylinder ( $u$  is the linear sliding speed of the rotating ring).

$u$ (m/s)	0.02	0.05	0.07	0.13	0.18	0.4	0.66
$h_0$ (m)	$4.44 \times 10^{-8}$	$8.44 \times 10^{-8}$	$1.06 \times 10^{-7}$	$1.64 \times 10^{-7}$	$2.06 \times 10^{-7}$	$3.61 \times 10^{-7}$	$5.13 \times 10^{-7}$
$\lambda$	0.92	1.75	2.22	3.42	4.30	7.53	10.69
Lubrication condition	BL	ML	ML	EL	EL	HL	HL
Hersey number	$8.08 \times 10^{-7}$	$1.77 \times 10^{-6}$	$2.91 \times 10^{-6}$	$4.50 \times 10^{-6}$	$6.26 \times 10^{-6}$	$1.39 \times 10^{-5}$	$2.26 \times 10^{-5}$

**Table 7.** Characteristics of lubrication film for polyalphaolefin 8 + 1 wt. % additive based on the velocity of the cylinder ( $u$  is the linear sliding speed of the rotating ring).

$u$ (m/s)	0.02	0.05	0.07	0.13	0.18	0.4	0.66
$h_0$ (m)	$4.66 \times 10^{-8}$	$8.84 \times 10^{-8}$	$1.11 \times 10^{-7}$	$1.72 \times 10^{-7}$	$2.16 \times 10^{-7}$	$3.79 \times 10^{-7}$	$5.38 \times 10^{-7}$
$\lambda$	0.96	1.84	2.33	3.59	4.51	7.89	11.21
Lubrication condition	BL	ML	ML	EL	EL	HL	HL
Hersey number	$8.64 \times 10^{-7}$	$1.89 \times 10^{-6}$	$2.87 \times 10^{-6}$	$4.81 \times 10^{-6}$	$6.70 \times 10^{-6}$	$1.49 \times 10^{-5}$	$2.42 \times 10^{-5}$

### 3.4. Wear Track Analysis

The assessment of wear degradation of the samples after tribological testing (refer to Table 8) was conducted by utilization of optical microscopy. Given the inherent difficulty in quantifying wear for DLC coatings due to their high wear resistance, wear track images obtained through optical microscopy were subject to comparative evaluation. At lower sliding speeds, the lubrication regime transitions into the BL or ML regime, potentially leading to direct surface-to-surface contact and the formation of localized wear scars on the confronting surfaces. As inferred from the calculations shown in Tables 6 and 7, the lubrication condition shifts to a BL or ML state at lower velocities. This shift may lead to direct surface-to-surface contact, ultimately leading to the degradation on confronting surfaces. When comparing results for the same coating before and after the addition of IL into PAO 8, a noticeable reduction in wear is evident across all thin films. However, drawing clear comparisons among these films when used with IL is not straightforward based solely on this technique [2].

**Table 8.** Optical microscopy photos of various lubricated films.

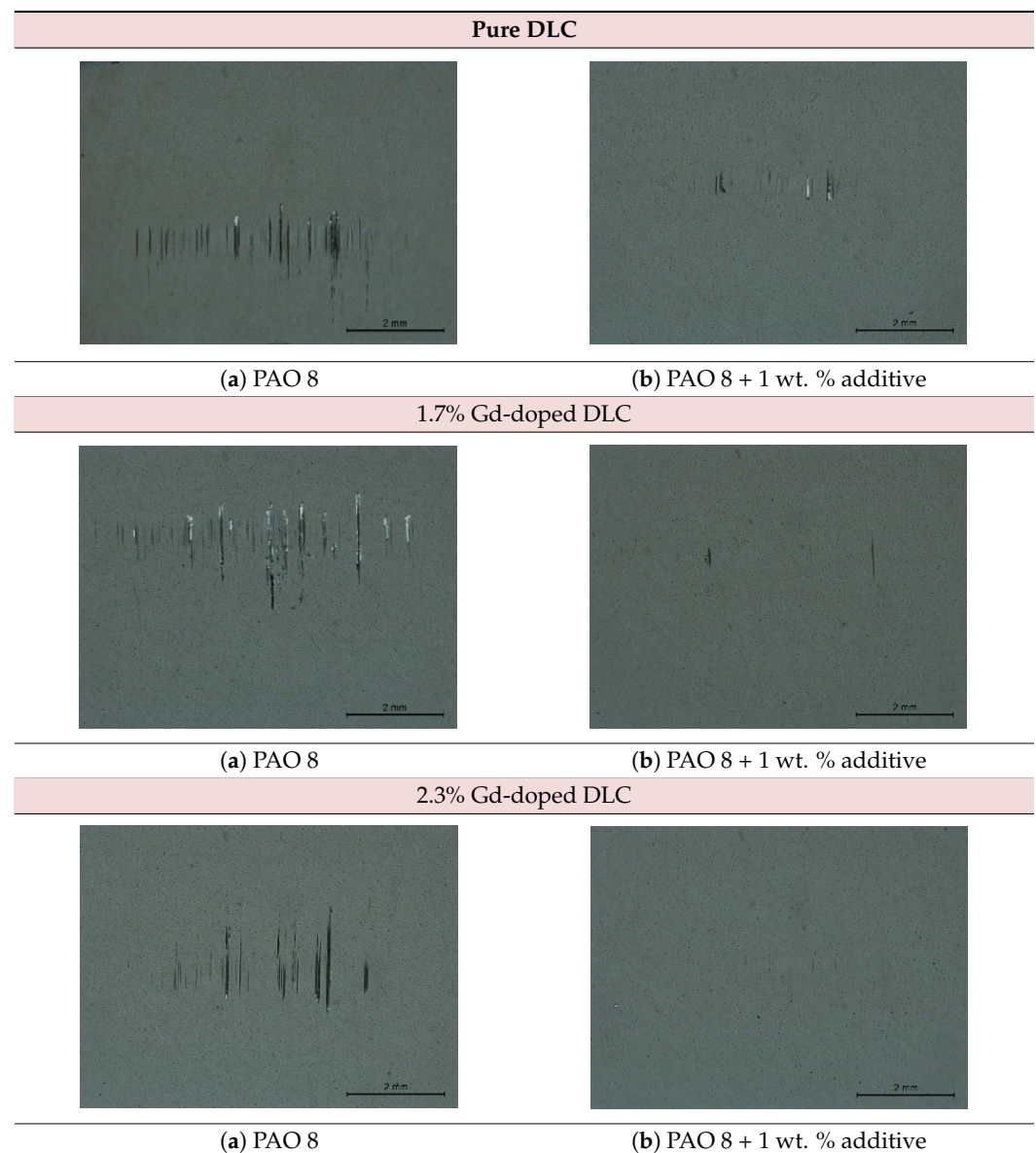
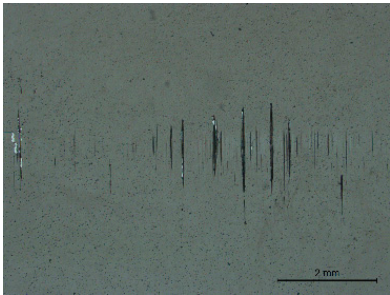
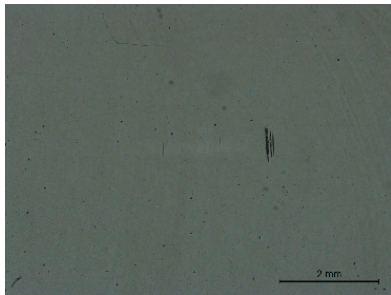
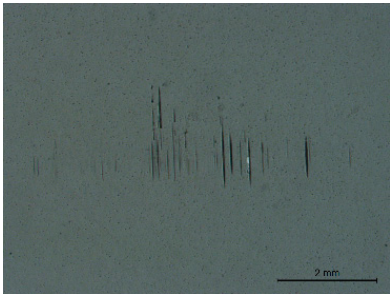
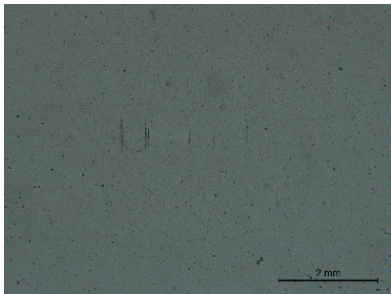
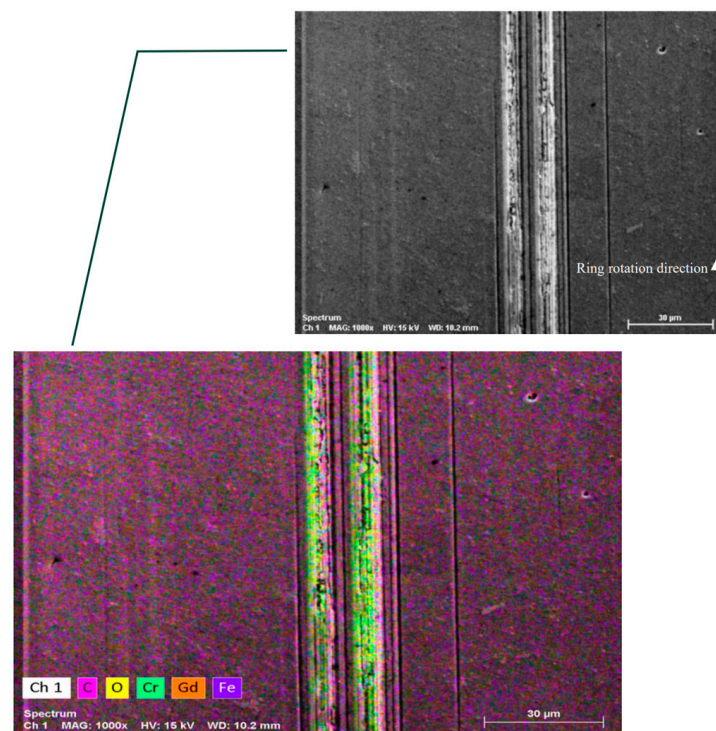


Table 8. Cont.

Pure DLC	
1.7% Eu-doped DLC	
	
(a) PAO 8	(b) PAO 8 + 1 wt. % additive
2.4% Ed-doped DLC	
	
(a) PAO 8	(b) PAO 8 + 1 wt. % additive

### 3.5. SEM/EDS Analysis

SEM and EDS were employed to assess the impact of using ionic liquid additives on coatings. However, this technique proves inadequate for effectively identifying the development of a tribofilm in this context. Its limitations lie in its inability to provide insights into chemical bonding; it solely provides elemental information. Consequently, employing more advanced methods for detecting chemical structures (for instance, ToF-SIMS or NR analysis) would be preferable for disclosing the development of the tribofilm. Within this section, exclusively, the outcomes for doped DLCs with lower atomic concentrations of dopant elements are provided (Figures 8–11). In the situation of the 1.7% Gd-doped DLC coating combined with polyalphaolefin 8 + 1 wt. % additive, there are areas where the DLC layer has been removed, revealing the presence of chromium which comes from the interlayer. Additionally, traces of oxygen are found on the worn tracks, indicating the development of oxide layers on the worn surface. Iron is not detected in the worn tracks which indicates that the interlayer has not been completely removed (because iron is only present in the substrate). In the scenario involving the 1.7% Eu-doped DLC coating along with polyalphaolefin 8 + 1 wt. % additive, certain areas exhibit a lack of the diamond-like carbon coating, exposing chromium from the interlayer. Furthermore, hints of oxygen are identified on the worn pathways, suggesting the development of oxides on the worn sections. The fact that iron is not detectable in the worn tracks implies that the interlayer has not been completely eliminated [2].



**Figure 8.** Top image depicts the SEM image of the 1.7% Gd-doped DLC surface combined with polyalphaolefin 8 + 1 wt. % additive without revealing elements post the tribology test. Bottom image represents the elemental analysis of the top image, captured through EDS methodology (25 N applied load and after 0.02 m/s sliding speed test).

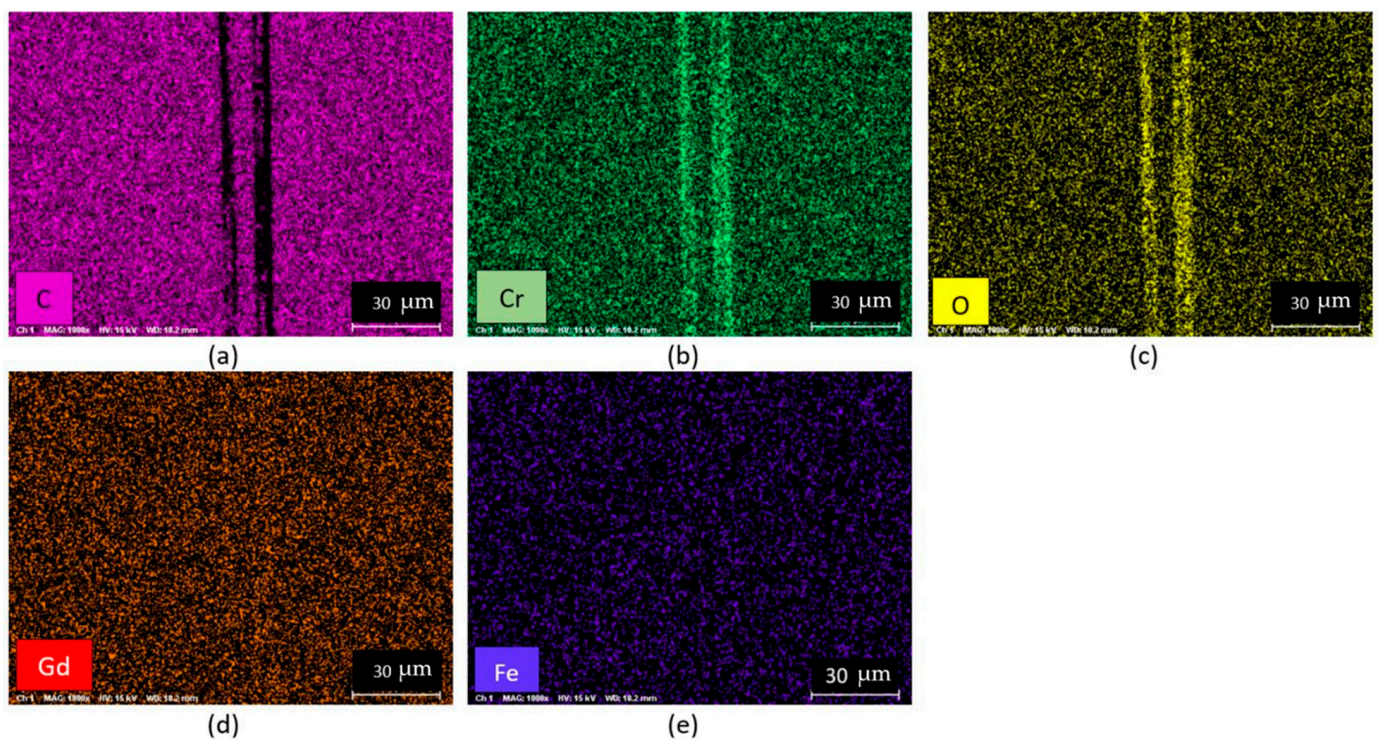


**Figure 9.** Element mapping of the 1.7% Gd-doped DLC coating combined with polyalphaolefin 8 + 1 wt. % additive following the tribology test: (a) carbon; (b) chromium; (c) oxygen; (d) gadolinium; (e) iron (analyzed using EDS technique).

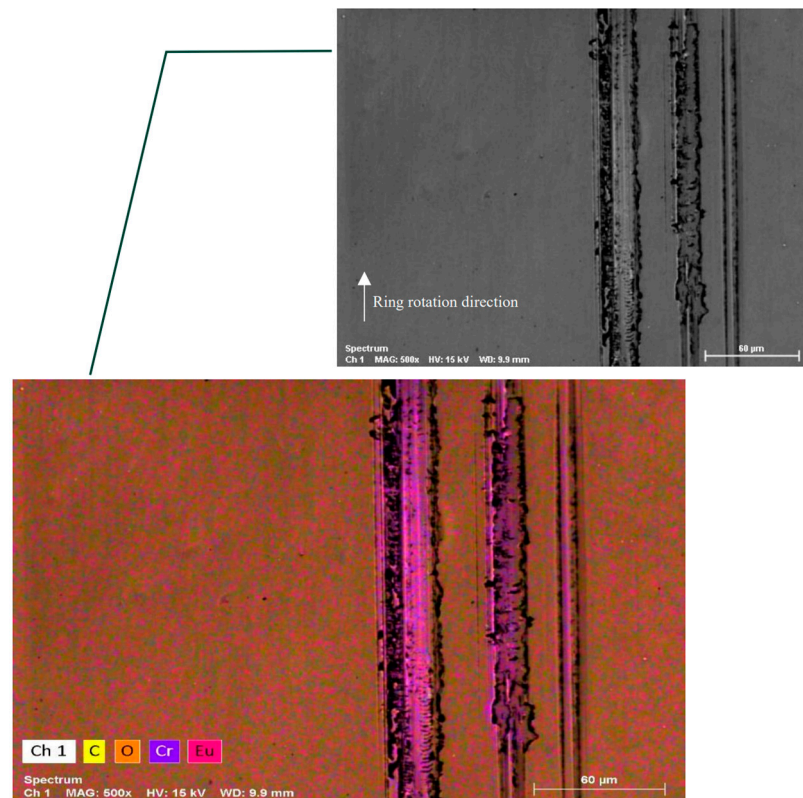


**Figure 10.** Top image displays the SEM image of the 1.7% Eu-doped DLC surface in conjunction with polyalphaolefin 8 + 1 wt. % additive, excluding elements observed after the tribology test. Bottom image depicts the elemental analysis of the top image, captured through EDS methodology (25 N applied load and after 0.02 sliding speed test).

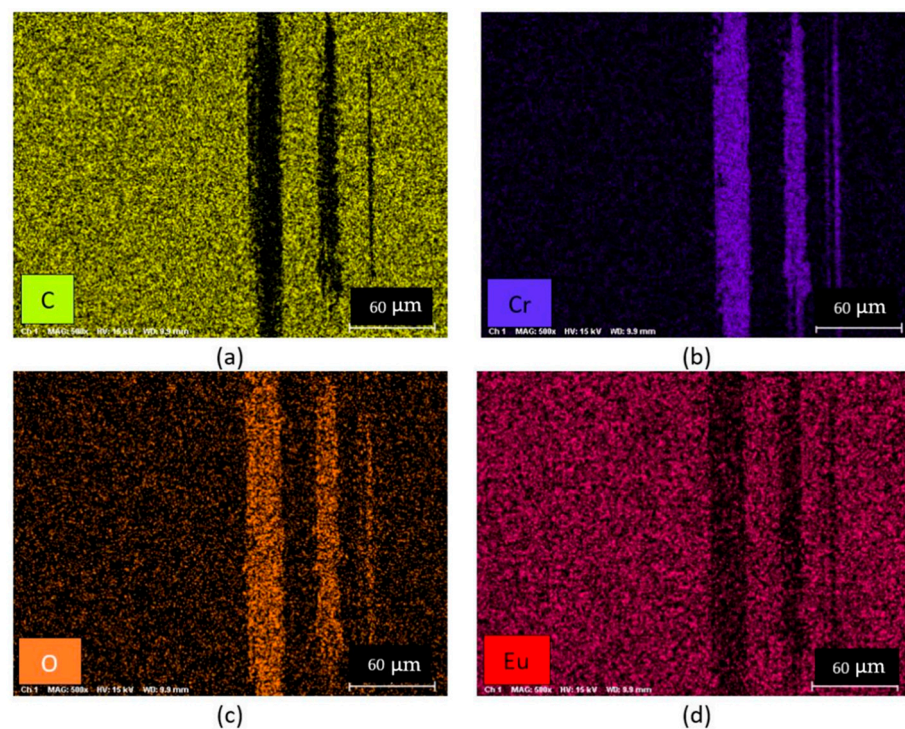


**Figure 11.** Element mapping of the 1.7% Eu-doped DLC coating combined with polyalphaolefin 8 + 1 wt. % additive following the tribology experiment: (a) carbon; (b) chromium; (c) oxygen; (d) europium (analyzed using EDS equipment).

#### 4. Conclusions

The present investigation concentrated on assessing the influence of incorporating 1 wt. % of the additive 1-Ethyl-3-methylimidazolium diethylphosphate ionic liquid into the PAO8 lubricant. This was conducted in lubricated pairs involving AISI 3415 steel coated with five distinct DLC coatings (specifically, 1.7% Gd-doped DLC, 2.3% Gd-doped DLC, 1.7% Eu-doped DLC, 2.4% Eu-doped DLC, and pure DLC films). The following key observations can be inferred from this study:

1. Among the five coatings examined, the 1.7% Gd-doped DLC coating displayed the highest hardness value. While 1.7% Gd-DLC, 1.7% Eu-DLC, and 2.4% Eu-DLC showed almost similar  $I_D/I_G$  values, 2.3% Gd-DLC has the highest  $I_D/I_G$  value which corresponds to lower percentage of  $sp^3$  content in its structure.
2. In scenarios where PAO8 served as the primary lubricant without added ionic liquids, the pure diamond-like carbon film demonstrated the least friction when interacting with the opposing surface.
3. Upon the addition of 1 wt. % of ionic liquid additive to PAO8, a noteworthy reduction in the CoF was observed across all lubrication conditions for the 1.7% Eu-doped DLC coating, outperforming all other pairs.

While the measurement of wear degradation posed challenges, a comparison of wear scars, based on images obtained through optical microscopy, between PAO8 without additives and polyalphaolefin 8 + 1 wt. % IL additive revealed a significant reduction in wear for all coatings. Nevertheless, due to limitations in scientifically proven wear measurement methods, a precise quantitative comparison of wear among these five films in the presence of IL additive could not be achieved.

**Author Contributions:** Conceptualization, F.F. (Fábio Ferreira) and A.R.; methodology, F.F. (Fábio Ferreira) and A.R.; formal analysis, M.S., T.O. and L.V.; investigation, M.S. and L.V.; resources, F.F. (Fábio Ferreira) and A.R.; writing—original draft preparation, M.S. and F.F. (Filipe Fernandes); writing—review and editing, F.F. (Fábio Ferreira), T.O. and L.V.; supervision, F.F. (Filipe Fernandes) and F.F. (Fábio Ferreira); project administration, F.F. (Filipe Fernandes) and F.F. (Fábio Ferreira); funding acquisition, F.F. (Fábio Ferreira). All authors have read and agreed to the published version of the manuscript.

**Funding:** This research is sponsored by national funds through FCT—Fundação para a Ciência e a Tecnologia, under the project UIDB/00285/2020 and LA/P/0112/2020, LubEnergy (UTAP-EXPL/NPN/0046/2021), SmartHyLub (2022.05603.PTDC) and the Taiho Kogyo Tribology Research Foundation (Grant No. 22A25).

**Data Availability Statement:** Data are contained within the article.

**Conflicts of Interest:** The authors declare no conflicts of interest.

#### References

1. Reduce Friction, Save Energy-ITAINNOVA. Available online: <https://www.itainnova.es/blog/materiales/reduce-friction-save-energy/> (accessed on 14 January 2023).
2. Sadeghi, M.; Omiya, T.; Fernandes, F.; Vilhena, L.; Ramalho, A.; Ferreira, F. Tribological Behavior of Doped DLC Coatings in the Presence of Ionic Liquid Additive under Different Lubrication Regimes. *Coatings* **2023**, *13*, 891. [CrossRef]
3. Shaikh, S.; Omiya, T.; Cavaleiro, A.; Vilhena, L.; Ramalho, A.; Ferreira, F. Impact of Temperature Variation on Friction Behaviour of Rare Earth-Doped Diamond-like Carbon Coatings with Ionic Liquid Lubricants. *Lubricants* **2023**, *11*, 302. [CrossRef]
4. Omiya, T.; Fontes, M.; Vuchkov, T.; Cruz, S.; Cavaleiro, A.; Ferreira, F. Tribological Performance of Gd-DLC and Eu-DLC Coatings in the Presence of Synthetic Oils Containing Ionic Liquid Additives Keywords. *Tribol. Lett.* **2023**, *71*, 65. [CrossRef]
5. Khanmohammadi, H.; Wijanarko, W.; Cruz, S.; Evaristo, M.; Espallargas, N. Triboelectrochemical Friction Control of W- and Ag-Doped DLC Coatings in Water-Glycol with Ionic Liquids as Lubricant Additives. *RSC Adv.* **2022**, *12*, 3573–3583. [CrossRef]
6. Spikes, H. The History and Mechanisms of ZDDP. *Tribol. Lett.* **2004**, *17*, 469–489. [CrossRef]
7. Ren, S.; Zheng, S.; Pu, J.; Lu, Z.; Zhang, G. Study of Tribological Mechanisms of Carbon-Based Coatings in Antiwear Additive Containing Lubricants under High Temperature. *RSC Adv.* **2015**, *5*, 66426–66437. [CrossRef]
8. Ratoi, M.; Niste, V.B.; Zekonyte, J. WS2 Nanoparticles—Potential Replacement for ZDDP and Friction Modifier Additives. *RSC Adv.* **2014**, *4*, 21238–21245. [CrossRef]

9. Fontes, M.A.; Serra, R.G.H.; Fernandes, F.D.; Cavaleiro Rodrigues de Carvalho, A.A.; de Sousa Ferreira, F.E. Comparison of Mechanical and Tribological Properties of Diamond-like Carbon Coatings Doped with Europium and Gadolinium Produced by HiPIMS. *Proc. Inst. Mech. Eng. B J. Eng. Manuf.* **2022**, 09544054221136528. [[CrossRef](#)]
10. Zhao, F.; Li, H.; Ji, L.; Wang, Y.; Zhou, H.; Chen, J. Ti-DLC Films with Superior Friction Performance. *Diam. Relat. Mater.* **2010**, *19*, 342–349. [[CrossRef](#)]
11. Ming, M.Y.; Jiang, X.; Piliptsov, D.G.; Zhuang, Y.; Rogachev, A.V.; Rudenkov, A.S.; Balmakou, A. Chromium-Modified a-C Films with Advanced Structural, Mechanical and Corrosive-Resistant Characteristics. *Appl. Surf. Sci.* **2016**, *379*, 424–432. [[CrossRef](#)]
12. Balestra, R.M.; Castro, A.M.G.; Evaristo, M.; Escudeiro, A.; Mutafov, P.; Polcar, T.; Cavaleiro, A. Carbon-Based Coatings Doped by Copper: Tribological and Mechanical Behavior in Olive Oil Lubrication. *Surf. Coat. Technol.* **2011**, *205*, S79–S83. [[CrossRef](#)]
13. Bhowmick, S.; Banerji, A.; Alpas, A.T. Tribological Behaviour of W-DLC against an Aluminium Alloy Subjected to Lubricated Sliding. *Tribol. Ind.* **2015**, *37*, 277–283.
14. Bociaga, D.; Komorowski, P.; Batory, D.; Szymanski, W.; Olejnik, A.; Jastrzebski, K.; Jakubowski, W. Silver-Doped Nanocomposite Carbon Coatings (Ag-DLC) for Biomedical Applications—Physiochemical and Biological Evaluation. *Appl. Surf. Sci.* **2015**, *355*, 388–397. [[CrossRef](#)]
15. Evaristo, M.; Polcar, T.; Cavaleiro, A. Tribological Behaviour of W-Alloyed Carbon-Based Coatings in Dry and Lubricated Sliding Contact. *Lubr. Sci.* **2014**, *26*, 428–439. [[CrossRef](#)]
16. Evaristo, M.; Fernandes, F.; Cavaleiro, A. Room and High Temperature Tribological Behaviour of W-DLC Coatings Produced by DCMS and Hybrid DCMS-HiPIMS Configuration. *Coatings* **2020**, *10*, 319. [[CrossRef](#)]
17. Majeed, S.; Siraj, K.; Naseem, S.; Khan, M.F.; Irshad, M.; Faiz, H.; Mahmood, A. Structural and Optical Properties of Gold-Incorporated Diamond-like Carbon Thin Films Deposited by RF Magnetron Sputtering. *Mater. Res Express* **2017**, *4*, 076403. [[CrossRef](#)]
18. Liu, N.; Zhu, H.; Wei, Q.; Long, H.; Deng, Z.; Yu, Z.; Xie, Y.; Wang, J.; Ma, L.; Zhou, K. A Niobium and Nitrogen Co-Doped DLC Film Electrode and Its Electrochemical Properties. *J Electrochem. Soc.* **2017**, *164*, H1091–H1098. [[CrossRef](#)]
19. Wang, L.; Jin, J.; Zhu, C.; Li, G.; Kuang, X.; Huang, K. Effects of HiPIMS Pulse-Length on Plasma Discharge and on the Properties of WC-DLC Coatings. *Appl. Surf. Sci.* **2019**, *487*, 526–538. [[CrossRef](#)]
20. Zia, A.W.; Zhou, Z.; Li, L.K.-Y. Structural, Mechanical, and Tribological Characteristics of Diamond-like Carbon Coatings. In *Nanomaterials-Based Coatings*; Nguyen Tri, P., Rtimi, S., Ouellet Plamondon, C.M., Eds.; Elsevier: Amsterdam, The Netherlands, 2019; pp. 171–194, ISBN 978-0-12-815884-5.
21. Zhang, R.; Wang, L. Synergistic Improving of Tribological Properties of Amorphous Carbon Film Enhanced by F–Si-Doped Multilayer Structure under Corrosive Environment. *Surf. Coat. Technol.* **2015**, *276*, 626–635. [[CrossRef](#)]
22. Zhang, S.; Yan, M.; Yang, Y.; Zhang, Y.; Yan, F.; Li, H. Excellent Mechanical, Tribological and Anti-Corrosive Performance of Novel Ti-DLC Nanocomposite Thin Films Prepared via Magnetron Sputtering Method. *Carbon N. Y.* **2019**, *151*, 136–147. [[CrossRef](#)]
23. Jo, Y.J.; Zhang, T.F.; Son, M.J.; Kim, K.H. Synthesis and Electrochemical Properties of Ti-Doped DLC Films by a Hybrid PVD/PECVD Process. *Appl. Surf. Sci.* **2018**, *433*, 1184–1191. [[CrossRef](#)]
24. Rana, R.; Walia, R.S.; Murtaza, Q. Characterization and Parametric Optimization of Performance Parameters of DLC-Coated Tungsten Carbide (WC) Tool Using TOPSIS. *Coatings* **2021**, *11*, 760. [[CrossRef](#)]
25. Liu, L.; Huang, J.; He, X.; Wang, T.; He, Z.; Du, K.; Diao, X. Preparation and Characterization of High Quality Diamond like Carbon Films on Si Microspheres. *Mater. Lett* **2018**, *220*, 309–312. [[CrossRef](#)]
26. Sharifahmadian, O.; Mahboubi, F.; Yazdani, S. Comparison between Corrosion Behaviour of DLC and N-DLC Coatings Deposited by DC-Pulsed PACVD Technique. *Diam. Relat. Mater.* **2019**, *95*, 60–70. [[CrossRef](#)]
27. Carvalho, I.; Dias, N.; Henriques, M.; Calderon, V.S.; Ferreira, P.; Cavaleiro, A.; Carvalho, S. Antibacterial Effects of Bimetallic Clusters Incorporated in Amorphous Carbon for Stent Application. *ACS Appl. Mater. Interfaces* **2020**, *12*, 24555–24563. [[CrossRef](#)]
28. Antunes, J.; Matos, K.; Carvalho, I.; Carvalho, S.; Ferreira, F.; Cruz, S.M.A. Physical Vapor Deposition Technology in Personal Protective Equipment Production: Improved Antibacterial and Hydrophobic Character of Textiles. *Coatings* **2022**, *12*, 1399. [[CrossRef](#)]
29. Zhou, F.; Liang, Y.; Liu, W. Ionic Liquid Lubricants: Designed Chemistry for Engineering Applications. *Chem. Soc. Rev.* **2009**, *38*, 2590–2599. [[CrossRef](#)]
30. Ye, C.; Liu, W.; Chen, Y.; Yu, L. Room-Temperature Ionic Liquids: A Novel Versatile Lubricant. *Chem. Commun.* **2001**, 2244–2245. [[CrossRef](#)]
31. Nanao, H.; Takahashi, K.; Shirai, M. Lubricity Improvement of Imidazolium Cation-Based Ionic Liquids Treated with Carbon Dioxide. *J. Jpn. Pet. Inst.* **2017**, *60*, 329–332. [[CrossRef](#)]
32. Milewski, K.; Kudliński, J.; Madej, M.; Ozimina, D.; Kudliński -Trzuskawica, J.; Madej, P.M. The Interaction between Diamond like Carbon (DLC) Coatings and Ionic Liquids under Boundary Lubrication Conditions. *55 METALURGIJA* **2017**, *56*, 55–58.
33. González, R.; Battez, A.H.; Viesca, J.L.; Higuera-Garrido, A.; Fernández-González, A. Lubrication of DLC Coatings with Two Tris(Pentafluoroethyl)Trifluorophosphate Anion-Based Ionic Liquids. *Tribol. Trans.* **2013**, *56*, 887–895. [[CrossRef](#)]
34. Shahid Arshad, M.; Čoga, L.; Geue, T.; Kovač, J.; Cruz, S.M.A.; Kalin, M. Adsorption Mechanism of Tributylmethylphosphonium Dimethylphosphate Ionic Liquid on Diamond-like Carbon Coatings: Neutron Reflectometry Study. *Tribol. Int.* **2021**, *151*, 106482.

35. Arshad, M.S.; Kovač, J.; Cruz, S.; Kalin, M. Physicochemical and Tribological Characterizations of WDLC Coatings and Ionic-Liquid Lubricant Additives: Potential Candidates for Low Friction under Boundary-Lubrication Conditions. *Tribol. Int.* **2020**, *151*, 106482. [CrossRef]
36. Stoy, L.; Xu, J.; Kulkarni, Y.; Huang, C.-H. Ionic Liquid Recovery of Rare-Earth Elements from Coal Fly Ash: Process Efficiency and Sustainability Evaluations. *ACS Sustain. Chem. Eng.* **2022**, *10*, 11824–11834. [CrossRef]
37. Mishra, B.B.; Devi, N. Application of Bifunctional Ionic Liquids for Extraction and Separation of Eu<sup>3+</sup> from Chloride Medium. *Trans. Nonferrous Met. Soc. China* **2022**, *32*, 2061–2070. [CrossRef]
38. Grill, A. Diamond-like Carbon: State of the Art. *Diam. Relat. Mater.* **1999**, *8*, 428–434. [CrossRef]
39. Turanov, A.N.; Karandashev, V.K.; Boltoeva, M. Solvent Extraction of Intra-Lanthanides Using a Mixture of TBP and TODGA in Ionic Liquid. *Hydrometallurgy* **2020**, *195*, 105367. [CrossRef]
40. Bolander, N.W.; Steenwyk, B.D.; Sadeghi, F.; Gerber, G.R. Lubrication Regime Transitions at the Piston Ring-Cylinder Liner Interface. *Proc. Inst. Mech. Eng. Part J J. Eng. Tribol.* **2005**, *219*, 19–31. [CrossRef]
41. Vahidi, A.; Fonseca, D.; Oliveira, J.; Cavaleiro, A.; Ramalho, A.; Ferreira, F. Advanced Tribological Characterization of DLC Coatings Produced by Ne-Hipims for the Application on the Piston Rings of Internal Combustion Engines. *Appl. Sci.* **2021**, *11*, 10498. [CrossRef]
42. Pusterhofer, M.; Summer, F.; Wuketich, D.; Grün, F. Development of a Model Test System for a Piston Ring/Cylinder Liner-Contact with Focus on near-to-Application Seizure Behaviour. *Lubricants* **2019**, *7*, 104. [CrossRef]
43. Hu, Z. Chapter 6—Characterization of Materials, Nanomaterials, and Thin Films by Nanoindentation. In *Microscopy Methods in Nanomaterials Characterization*; Thomas, S., Thomas, R., Zachariah, A.K., Mishra, R.K., Eds.; Elsevier: Amsterdam, The Netherlands, 2017; pp. 165–239, ISBN 978-0-323-46141-2.
44. Sharma, S. *Tribological Behaviour of Laser Treated C-Alloyed TMD Coatings in Rubber Contact Effects of Protein on Tribocorrosion Behavior of Ti-6Al-4V. View Project Construction of Tribocorrosion Setup and Study the Degradation of Ti-Implants View Project*; University of Coimbra: Coimbra, Portugal, 2021.
45. Zhou, X.; Tunmee, S.; Suzuki, T.; Phothongkam, P.; Kanda, K.; Komatsu, K.; Kawahara, S.; Ito, H.; Saitoh, H. Quantitative NEXAFS and Solid-State NMR Studies of Sp<sup>3</sup>/(Sp<sup>2</sup>+sp<sup>3</sup>) Ratio in the Hydrogenated DLC Films. *Diam. Relat. Mater.* **2017**, *73*, 232–240. [CrossRef]
46. Gurbich, A.F. SigmaCalc Recent Development and Present Status of the Evaluated Cross-Sections for IBA. *Nucl. Instrum. Methods Phys. Res. B* **2016**, *371*, 27–32. [CrossRef]
47. ASTM G77-17; Standard Test Method for Ranking Resistance of Materials to Sliding Wear Using Block-on-Ring Wear Test. ASTM International: West Conshohocken, PA, USA, 2022. Available online: <https://www.astm.org/g0077-17.html> (accessed on 4 January 2024).
48. Cardoso, F.; Ferreira, F.; Cavaleiro, A.; Ramalho, A. Performance of Diamond-like Carbon Coatings (Produced by the Innovative Ne-HiPIMS Technology) under Different Lubrication Regimes. *Wear* **2021**, *477*, 203775. [CrossRef]
49. Luo, Q. Electron Microscopy and Spectroscopy in the Analysis of Friction and Wear Mechanisms. *Lubricants* **2018**, *6*, 58. [CrossRef]
50. Ferreira, F.; Serra, R.; Cavaleiro, A.; Oliveira, J.C. Additional Control of Bombardment by Deep Oscillation Magnetron Sputtering: Effect on the Microstructure and Topography of Cr Thin Films. *Thin Solid Films* **2016**, *619*, 250–260. [CrossRef]
51. Ferreira, F.; Aijaz, A.; Kubart, T.; Cavaleiro, A.; Oliveira, J. Hard and Dense Diamond like Carbon Coatings Deposited by Deep Oscillations Magnetron Sputtering. *Surf. Coat. Technol.* **2018**, *336*, 92–98. [CrossRef]
52. Lin, J.; Zhang, X.; Lee, P.; Wei, R. Thick Diamond like Carbon Coatings Deposited by Deep Oscillation Magnetron Sputtering. *Surf. Coat. Technol.* **2017**, *315*, 294–302. [CrossRef]
53. Hatem, A.; Lin, J.; Wei, R.; Torres, R.D.; Laurindo, C.; Soares, P. Tribocorrosion Behavior of DLC-Coated Ti-6Al-4V Alloy Deposited by PIID and PEMS+PIID Techniques for Biomedical Applications. *Surf. Coat. Technol.* **2017**, *332*, 223–232. [CrossRef]
54. Sharifahmadian, O.; Mahboubi, F.; Oskouie, A. Structural Evolution and Tribological Behavior of Nitrogen-Doped DLC Coatings Deposited by Pulsed DC PACVD Method. *Diam. Relat. Mater.* **2019**, *91*, 74–83. [CrossRef]
55. Kubart, T.; Aijaz, A.; Andersson, J.; Ferreira, F.; Oliveira, J.C.; Sobetskii, A.; Parau, A.C.; Vitelaru, C. High Power Impulse Magnetron Sputtering of Diamond-like Carbon Coatings. *J. Vac. Sci. Technol. A* **2020**, *38*, 043408. [CrossRef]
56. Serra, R.; Ferreira, F.; Cavaleiro, A.; Oliveira, J.C. HiPIMS Pulse Shape Influence on the Deposition of Diamond-like Carbon Films. *Surf. Coat. Technol.* **2022**, *432*, 128059. [CrossRef]
57. Kashyap, A.; Harsha, A.P.; Kondaiah, P.; Barshilia, H.C. Study on Galling Behaviour of HiPIMS Deposited Mo/DLC Multilayer Coatings at Ambient and Elevated Temperature. *Wear* **2022**, *498–499*, 204327. [CrossRef]
58. Ferrari, A.C.; Libassi, A.; Tanner, B.K.; Stolojan, V.; Yuan, J.; Brown, L.M.; Rodil, S.E.; Kleinsorge, B.; Robertson, J. Density, Sp<sup>3</sup> Fraction, and Cross-Sectional Structure of Amorphous Carbon Films Determined by x-Ray Reflectivity and Electron Energy-Loss Spectroscopy. *Phys. Rev. B* **2000**, *62*, 11089–11103. [CrossRef]
59. Foong, Y.M.; Hsieh, J.; Li, X.; Chua, D.H.C. Comparative Study between Erbium and Erbium Oxide-Doped Diamondlike Carbon Films Deposited by Pulsed Laser Deposition Technique. *J. Vac. Sci. Technol. A* **2010**, *28*, 449–455. [CrossRef]
60. Schmidt, K.; Laumer, J.; O’Leary, S.K. The D- and G-Branched Associated with the Raman Spectrum of Thin-Film Carbon. *Solid State Commun.* **2023**, *360*, 115041. [CrossRef]
61. Vetter, J. 60years of DLC Coatings: Historical Highlights and Technical Review of Cathodic Arc Processes to Synthesize Various DLC Types, and Their Evolution for Industrial Applications. *Surf. Coat. Technol.* **2014**, *257*, 213–240. [CrossRef]

62. Liu, Y.; Erdemir, A.; Meletis, E.I. A Study of the Wear Mechanism of Diamond-like Carbon Films. *Surf. Coat. Technol.* **1996**, *82*, 48–56. [[CrossRef](#)]
63. Robertson, J. Diamond-like Amorphous Carbon. *Mater. Sci. Eng. R Rep.* **2002**, *37*, 129–281. [[CrossRef](#)]
64. Ding, J.C.; Mei, H.; Jeong, S.; Zheng, J.; Wang, Q.M.; Kim, K.H. Effect of Bias Voltage on the Microstructure and Properties of Nb-DLC Films Prepared by a Hybrid Sputtering System. *J. Alloys Compd.* **2021**, *861*, 158505. [[CrossRef](#)]
65. Ding, J.C.; Chen, M.; Mei, H.; Jeong, S.; Zheng, J.; Yang, Y.; Wang, Q.; Kim, K.H. Microstructure, Mechanical, and Wettability Properties of Al-Doped Diamond-like Films Deposited Using a Hybrid Deposition Technique: Bias Voltage Effects. *Diam. Relat. Mater.* **2022**, *123*, 108861. [[CrossRef](#)]
66. Wang, Y.; Wang, Q.J. Stribeck Curves. In *Encyclopedia of Tribology*; Wang, Q.J., Chung, Y.-W., Eds.; Springer: Boston, MA, USA, 2013; pp. 3365–3370, ISBN 978-0-387-92897-5.
67. Marinescu, I.D.; Rowe, W.B.; Dimitrov, B.; Inasaki, I. Process Fluids for Abrasive Machining. In *Tribology of Abrasive Machining Processes*; Marinescu, I.D., Rowe, W.B., Dimitrov, B., Inasaki, I., Eds.; William Andrew Publishing: Norwich, NY, USA, 2004; pp. 531–585, ISBN 978-0-8155-1490-9.
68. Xin, Q. Friction and Lubrication in Diesel Engine System Design. In *Diesel Engine System Design*; Xin, Q., Ed.; Elsevier: Amsterdam, The Netherlands, 2013; pp. 651–758, ISBN 978-1-84569-715-0.
69. Kalin, M.; Velkavrh, I.; Vižintin, J. The Stribeck Curve and Lubrication Design for Non-Fully Wetted Surfaces. *Wear* **2009**, *267*, 1232–1240. [[CrossRef](#)]
70. Lu, X.; Khonsari, M.M.; Gelinck, E.R.M. The Stribeck Curve: Experimental Results and Theoretical Prediction. *J. Tribol.* **2006**, *128*, 789–794. [[CrossRef](#)]
71. Wang, Y.; Wang, Q.J.; Lin, C.; Shi, F. Development of a Set of Stribeck Curves for Conformal Contacts of Rough Surfaces. *Tribol. Trans.* **2006**, *49*, 526–535. [[CrossRef](#)]
72. Kalin, M.; Velkavrh, I. Non-Conventional Inverse-Stribeck-Curve Behaviour and Other Characteristics of DLC Coatings in All Lubrication Regimes. *Wear* **2013**, *297*, 911–918. [[CrossRef](#)]
73. Martini, A.; Zhu, D.; Wang, Q. Friction Reduction in Mixed Lubrication. *Tribol. Lett.* **2007**, *28*, 139–147. [[CrossRef](#)]
74. Kajdas, C. Importance of Anionic Reactive Intermediates for Lubricant Component Reactions with Friction Surfaces. *Lubr. Sci.* **1994**, *6*, 203–228. [[CrossRef](#)]
75. Xiao, H. Ionic Liquid Lubricants: Basics and Applications. *Tribol. Trans.* **2017**, *60*, 20–30. [[CrossRef](#)]
76. Atkin, R.; el Abedin, S.Z.; Hayes, R.; Gasparotto, L.H.S.; Borisenko, N.; Endres, F. AFM and STM Studies on the Surface Interaction of [BMP]TFSA and [EMIm]TFSA Ionic Liquids with Au(111). *J. Phys. Chem. C* **2009**, *113*, 13266–13272. [[CrossRef](#)]
77. Perkin, S.; Albrecht, T.; Klein, J. Layering and Shear Properties of an Ionic Liquid, 1-Ethyl-3-Methylimidazolium Ethylsulfate, Confined to Nano-Films between Mica Surfaces. *Phys. Chem. Chem. Phys.* **2010**, *12*, 1243–1247. [[CrossRef](#)]
78. Marian, M.; Bartz, M.; Wartzack, S.; Rosenkranz, A. Non-Dimensional Groups, Film Thickness Equations and Correction Factors for Elastohydrodynamic Lubrication: A Review. *Lubricants* **2020**, *8*, 95. [[CrossRef](#)]

**Disclaimer/Publisher’s Note:** The statements, opinions and data contained in all publications are solely those of the individual author(s) and contributor(s) and not of MDPI and/or the editor(s). MDPI and/or the editor(s) disclaim responsibility for any injury to people or property resulting from any ideas, methods, instructions or products referred to in the content.